This article has been accepted for publication in IEEE Transactions on Industrial Electronics. This is the author's version which has not been fully edited and content may change prior to final publication. Citation information: DOI 10.1109/TIE.2023.3262866

Towards Resiliency Enhancement of Network of Grid-Forming and Grid-Following Inverters

Silvanus D'silva, *Student Member*, *IEEE*, Alireza Zare, *Student Member*, *IEEE*, Mohammad B. Shadmand, *Senior Member, IEEE,* Sertac Bayhan*, Senior Member, IEEE,* Haitham Abu-Rub*, Fellow, IEEE*

***Abstract*— This paper proposes an autonomous control scheme to mitigate voltage-frequency excursions observed in a network of grid forming (GFM) and grid following (GFL) inverters in a power electronics dominated grid (PEDG). The proposed control scheme leverages GFL inverter's ability to dynamically adjust their power set-points as well as change their operation mode on-the-fly to enhance the PEDG resiliency. A supervisory controller (SC) comprising of a Droop-ΔP estimator coupled with an optimal power allocator (OPA) module dynamically adjusts the power injections from GFL inverters to maintain the power balance and restore frequency in response to disturbances. Moreover, the proposed self-ranking based coordinated mode selection (SR-CMS) algorithm dynamically reconfigures the inverter's operation mode (either GFM or GFL) to enhance the PEDG resiliency in response to events and ensure GFM inverter allocation in grid clusters. Several case studies are performed to validate the feasibility, performance, and robustness of proposed autonomous control. Finally, the proposed scheme is experimentally validated on a small-scale hardware testbed.**

***Keywords*– grid forming inverter, grid following inverter, frequency restoration, resiliency.**

I. Introduction

Current trends towards integration of renewable sources in the power system backed by the net-zero emissions goal of several governmental agencies has led to emergence of a power electronics dominated grid (PEDG) paradigm [1]. PEDG aims at transforming the conventional grid into an intricate network of inverter-based resources [2]. A typical PEDG is characterized by generation units located in close proximity to loads, uninterrupted power fed to local loads enhancing the system resiliency, dynamic islanding and reconnection abilities via multiple points of common coupling (PCC)s, inverter based voltage-frequency (*V-f*) restoration, etc. [3, 4]. On the contrary, PEDG has also introduced multiple challenges such as inherent lower inertia due to replacement of synchronous generators with inverters, need for complex multi-layered multi-timescale controllers, weather-related generation constraints, lower reactance-to-resistance (X/R) ratio and lower fault ride through capabilities [1]. Besides, the transformation from a centralized to distributed generation has also compromised the PEDG's security and made it vulnerable to potential anomalies [3, 4].

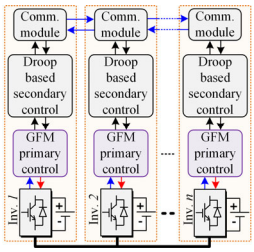
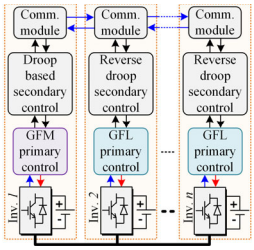
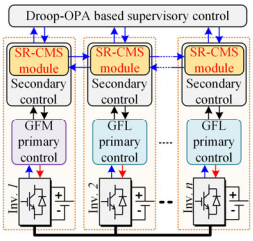
The resilient operation of PEDG is highly dependent upon DERs which are interfaced to the grid via inverters. The inverters in a PEDG are commonly operated in either (a) grid forming (GFM) or (b) grid following (GFL) modes. A GFM inverter is characterized by a controlled voltage source that regulates its output *V-f,* while a GFL inverter is characterized by a controlled current source that injects desired amount of active-reactive power when demanded by the network. The optimal dispatch set-points of GFL inverters are typically obtained from a supervisory controller (SC) [3, 4]. On the other hand, GFM inverters are supporting the *V-f* in the PEDG and typically providing virtual inertia to enhance the system resiliency. Multiple studies have been carried out in the literature to investigate the enhancement of V-f dynamic response by selecting proper mode of inverter operation i.e. GFM versus GFL mode. The strategic placement of GFM and GFL inverters enhances the *V-f* dynamic response, demand-supply stability, and inertial response of the PEDG [5]. Various studies have also explored that advanced functions such as damping [6] and virtual inertia emulation [7] via a fleet of GFM inverters enhance the system's stability. However, a PEDG network containing 100% GFM inverters may introduce its own set of challenges related to synchronization, circulating reactive powers, unregulated power sharing, etc. as each GFM tries to regulate the network's *V-f* [8]. On the contrary, at least one GFM inverter is essential in each cluster in PEDG with islanding capability to maintain slack bus crucial for synchronization of GFL inverters within the cluster boundaries and ensure required inertia emulation. This paper considers a PEDG islanded cluster with at least one GFM inverter interacting with several GFL inverters controlled by a multi-layered multi-time scale control scheme towards enhancing the resiliency of the network.

Various control approaches for network of GFM and GFL inverters in PEDG have been proposed in literature and are mainly classified as: centralized and distributed control schemes [3, 9, 10]; that can mitigate disturbance impacts to some extent. In centralized control approach, the satisfactory operation of the PEDG clusters heavily relies on a central SC which provides adequate power references to inverters along with vital protection features in the grid-connected and islanded modes [11, 12]. Various primary controllers for GFM and GFL inverters such as droop-based, virtual synchronous generator (VSG)-based, and virtual oscillator control (VOC)-based schemes are deployed in centralized control architecture where the SC provides the active-reactive power setpoints to these inverter's primary controllers to maintain system stability. However, in general the centralized control approach suffers from an inherent drawback related to single point of failure. Alternatively, distributed control approaches have been proposed in [13] where each inverter is equipped with a local coordinated controller in addition to the primary voltage or current controller, thereby eliminating SC's dependency. Each inverter that could be modeled as an agent interacts with its neighbors in a coordinated manner to attain the desired control objective. However, since agents only communicate with their neighbors, limited information about the entire cluster is

This work is licensed under a Creative Commons Attribution 4.0 License. For more information, see https://creativecommons.org/licenses/by/4.0/

This article has been accepted for publication in IEEE Transactions on Industrial Electronics. This is the author's version which has not been fully edited and content may change prior to final publication. Citation information: DOI 10.1109/TIE.2023.3262866

Table I. Comparison of state-of-the-art control schemes for resilient operation of GFM and GFL inverters in a PEDG

Method	Topology	Features	Drawbacks
Multiple Droop-based GFM only cluster [20-23]		• Minimal or no dependency on communication layer. • High modularity, flexibility and expandability. • Virtual inertial emulation capability.	• Multiple droop gain tuning challenges. • Synchronization of multiple GFM inverters is challenging. • Vulnerability to steep load disturbance due to lack of sufficient coordination. • Dependency on communication links for synchronization, adaptiveness, etc. • Can be implemented without communication in decentralized scheme at the cost of improper power sharing.
Single droop based GFM and multiple GFL based cluster [5, 13]		• Simple synchronization between single GFM and multiple GFL inverters. • Generation and load disturbances can be compensated by GFM and GFL inverters at different time scales. • In case of a GFL failure, GFM and other GFLs can adjust their power set point to maintain power balance.	• Vulnerable to single point of failure. • Failure or compromised GFM inverter will result in loss of slack bus and PCC V/f regulation is lost. • Lack of coordination between reverse-droop based GFLs and without considering their power reserve may results in fluctuations in V/f in response to disturbances. • Communication dependency. • No self-healing capability.
Proposed SR-CMS based GFM-GFL cluster		• Resilient to GFM failure or other single point of failures. • Simple synchronization between GFM, GFL inverters. • Optimal power sharing between all DERs considering their power reserve. • Minimal tuning effort for droop gains by minimizing the number of droop curves within the cluster. • Self-healing capability for determining the optimal next GFM candidate in response to failures. • Maximum resiliency and robustness with minimal communication requirement.	• Communication dependency.

available, which limits their performance compared to centralized schemes [14-17]. In summary, the above-mentioned control approaches adjust the GFL inverters' operation setpoints in a centralized or distributed manner to address the *V-f* fluctuations, provided all resources in the PEDG are available.

The missing piece of the puzzle here is what if an intentional or unintentional disturbance targets the PEDG resources, typically the GFM and GFL inverters. This paper aims at addressing this research gap to ensure resilient operation of PEDG clusters against *V-f* related disturbances. In a PEDG, such disturbances may arise due to a variety of reasons such as undesirable loss of load, generation loss due to insufficient incident solar irradiation, depleted state of charge (SoC) and state of health (SoH) of coupled battery energy storages (BESS) [18, 19], power stage failures, etc. thereby leading to power demand-supply imbalance. Furthermore, disturbances may also be introduced due to compromised or faulted GFM and GFL inverter controllers. Thus, a real-time fault resilient mechanism that can mitigate the catastrophic impacts of disturbances in the PEDGs *V-f* is required. This paper aims at addressing the associated *V-f* fluctuations regardless of the cause such as loss of the GFM or GFL inverter.

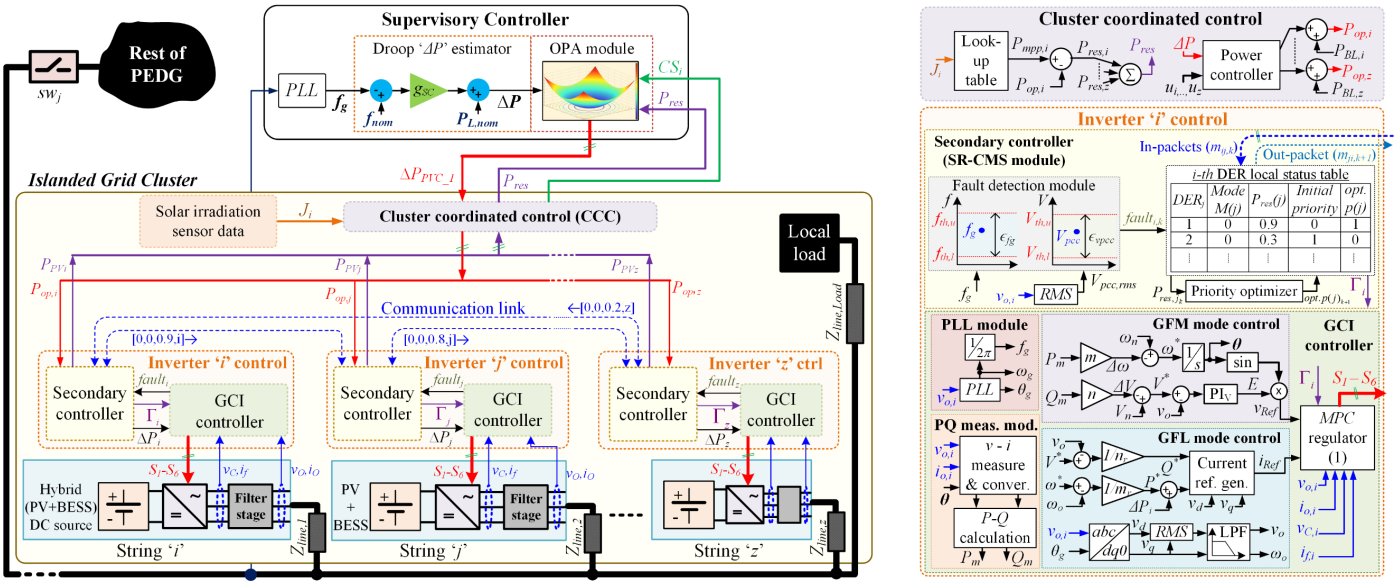
The proposed solution is based on an integrated centralized and distributed control framework that leverages the features of these two classes of control architecture for more resilient operation of the PEDG. Subsequently, this paper proposes a real-time autonomous control to restore the *V-f* in an islanded PEDG cluster consisting of one GFM inverter and multiple GFL inverters. The proposed approach uses a self-ranking based coordinated mode selection (SR-CMS) mechanism capable of dynamically reconfiguring inverter's operation mode to restore the PEDG and feed uninterrupted power to critical loads. Thus, the key contribution of this paper is:

- An integrated centralized and distributed control scheme for more resilient operation of PEDG,
- Real-time estimation of demanded power 'ΔP' and optimal power allocation among inverters to restore frequency,
- Self-reconfiguration of inverters operation modes within the cluster in response to loss of GFM inverters arising from failure of source, controller, power stage, etc.,
- Accurate power sharing amongst inverters thereby eliminating periodic reconfiguration of droop gains.

Furthermore, the superiority of the proposed control architecture is also compared with state-of-the-art droop-based control schemes. Table 1 shows the features and drawbacks of the state-of the-art control schemes for network of GFM and GFL inverters in PEDG and compared with the proposed SR-CMS based control scheme. These distributed control schemes can be categorized into GFM only [20-23] or combination of GFM and GFL inverters [5, 13] as summarized in Table 1. The remainder of the paper is structured as follows: Section II describes the PEDG and its various components along with the inverter's proposed controller architecture. Section III discusses the proposed SC comprising of Droop – ΔP estimation module and optimum power allocator (OPA) module. The proposed packet generation and coordinated mode selection mechanism is also discussed in this section. Section IV explains the simulation case studies' results. The results obtained from experimental hardware validation of the proposed SR-CMS scheme on a

This work is licensed under a Creative Commons Attribution 4.0 License. For more information, see https://creativecommons.org/licenses/by/4.0/

This article has been accepted for publication in IEEE Transactions on Industrial Electronics. This is the author's version which has not been fully edited and content may change prior to final publication. Citation information: DOI 10.1109/TIE.2023.3262866



(a) (b)

Fig. 1. Proposed self-ranking based coordinated mode selection (SR-CMS) control scheme for an islanded grid cluster (a). proposed system architecture and (b). inverter controllers.

small-scale testbed comprising of three inverters are discussed in section V. Finally, section VI concludes this paper.

II. System Overview

A. System Description

The architecture of the proposed islanded grid clusters in the PEDG is depicted in Fig. 1. The string inverters are connected at the cluster's PCC. The considered PEDG is divided into 'n' clusters, each containing 'z' string inverters that have dual operation mode and capable of switching between modes when demanded. Each string comprises of a source connected converter (SCC) cascaded with a grid connected dc-ac inverter (GCI); each equipped with its independent primary controllers as discussed in [24]. A cluster coordinated controller (CCC) governs the cluster's operation and serves as a local power dispatcher when the SC is faulted or compromised.

B. Grid Connected Inverter (GCI)

The detailed description of GCI that interfaces the hybrid dc source to the PCC is provided in [24]. As shown in Fig. 1.b, each GCI is driven by a model predictive controller (MPC) that uses the LCL filter's dynamic model [25] to minimize the cost function 'g'. The controller's cost function 'g' is given by,

$$g = \Gamma_i \left| v_{pcc}^{*} - v_{pcc,k+1} \right| + \left(1-\Gamma_i\right) \left| i_g^{*} - i_{g,k+1} \right| \tag{1}$$

where v_{pcc}^{*}, i_g^{*} indicate the output voltage's and grid current's reference values respectively while $v_{pcc,k+1}$, $i_{g,k+1}$ correspond to the next step predicted values for output voltage and grid current respectively. Next, Γ_i is a binary factor which determine the GCI's operation mode. In GFM mode, Γ_i is set to '1' and the GCI operates as a controlled voltage source while in GFL operation, Γ_i is set to '0' and the GCI operates in current controlled mode regulated by SC. Since the grid impedance in a PEDG is neither purely resistive nor inductive, the active and reactive power droop relations are not fully decoupled either. Thus, modified droop relations [26] that generate references for the GFM operation are given by,

$$f_g - f_0 = m_p\left(P - P_0\right) + n_q\left(Q - Q_0\right) \tag{2}$$

$$v_g - v_0 = m_p\left(P - P_0\right) - n_q\left(Q - Q_0\right) \tag{3}$$

where f_g, v_g represent the measured frequency and PCC voltage while f_0 , v_0 represent the nominal frequency and voltage respectively. $m_p = k_p\left(X_{line}/Z_{line}\right)$ and $n_q = k_q\left(R_{line}/Z_{line}\right)$ are the effective frequency and voltage droop gains respectively. The droop gains depend on ratio of resistive R_{line} and inductive line impedances X_{line} between two strings and $Z_{line} = \sqrt[2]{R_{line}^2 + X_{line}^2}$. P_0, Q_0 represent active and reactive powers of GCI in GFM respectively. Also, $P = P_m\left(\omega_c/(s+\omega_c)\right)$ and $Q = Q_m\left(\omega_c/(s+\omega_c)\right)$ are the measured active-reactive powers passed through a low pass filter of cut-off frequency ω_c.

C. Cluster coordinated control (CCC)

The CCC acts as the moderator between the SC and the SCC and GCI primary controllers. It determines the available power reserve in its strings based on the power output and the estimated maximum power; and conveys the total power reserve level to the SC. The maximum power is estimated using look-up tables using solar irradiation inputs given by $P_{mpp,s} = f\left(J_s\right)$. Here, $f(J_s)$ represents the look-up function discussed in [24]. Since all strings in a cluster are located nearby, the estimated $P_{mpp,s}$ coincides with the maximum generation ability. The instantaneous power reserve P_{res} in a cluster is given by,

$$P_{res} = \sum_{s=1}^{z}\left(P_{mpp,s} - P_{op,s}\right) \tag{4}$$

where $P_{op,s}$ is the s^{th} string output power. This value of P_{res} is send to SC to determine the next instance demanded power ΔP as discussed in Section III. Also, it assigns the power demand obtained from the SC to all connected strings. Thus, at any instance, the output power of a string s is given as base load P_{BLs} plus allocated demand ΔP_s in $P_s = P_{BL,s} + u * \Delta P_s$. Here, u is a binary operator set to '0' if string s is operating in GFM or is faulted; else it is set to '1' for GFL operation. Thus, the cluster's total harvested power P_k at instance k is given by,

This work is licensed under a Creative Commons Attribution 4.0 License. For more information, see https://creativecommons.org/licenses/by/4.0/

This article has been accepted for publication in IEEE Transactions on Industrial Electronics. This is the author's version which has not been fully edited and content may change prior to final publication. Citation information: DOI 10.1109/TIE.2023.3262866

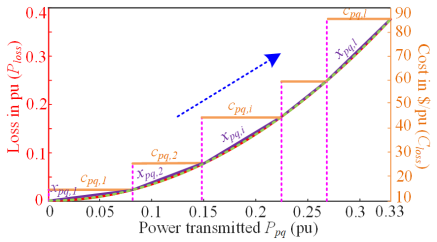


Fig. 2. Power transferred between strings p and q vs power loss vs loss cost.

$$P_k = \sum_{s=1}^{z} P_{s,k} = \sum_{s=1}^{z} \left(P_{BL,s_k} + \left(u * \Delta P_{sk} \right) \right) \tag{5}$$

III. Proposed Control Scheme

A. ΔP Estimator and Optimal Power Allocator (OPA)

A droop-based ΔP estimator coupled with OPA module in the SC is deployed to restore the frequency in a timely manner; particularly during load disturbances. The ΔP estimator determines the demanded power to maintain frequency f_g by,

$$\Delta P = P_0 - P_g = g_{SC}\left(f_g - f_0 \right) \tag{6}$$

where ΔP is the differential power required to restore the frequency f_g to nominal f_0. P_0 is nominal load while P_g is the PEDG's currently served load. Also, g_{SC} is the SC's gain.

The OPA module uses a convex optimization-based linear programming (LP) module to minimize power loss through incurred loss cost while ensuring system stability. Detailed analysis of the OPA module is provided in [24]. Consequently, the power loss incurred during power transfer from string p to string q is given by red curve in Fig. 2, which is translated to a loss cost curve represented by dotted green curve. For ease in formulation, power transferred from string p to q is approximated by linear piecewise function of l segments bearing generation rate $x_{pq,l}$. This function is represented by the purple plot. Thus, equality constraints for LP are given by,

$$\Delta P_{pq} = \sum_{i=1}^{l} x_{pq,i} \; ; i = (1,2,...,l) \; ; q = (1,2,...,z) \tag{7}$$

Also, the lower limit and higher limits $X_{pq,i}^{max}$ for all l segments provide the inequality constraints given by,

$$0 \le x_{pq,i} \le X_{pq,i}^{\max} \;\; ; \; i = (1,2,...,l) \tag{8}$$

Next, a cost factor $c_{pq,i}$ is assigned to each segment illustrated by horizontal orange segments in Fig. 2. The values assigned to $c_{pq,i}$ depend on the line impedances, loading profiles, etc. The generation uncertainties are incorporated in the cost function using a factor $b_{pq,i}$ with value ranging from 0.0 to 1.0 depending on incident solar irradiation. The power constraints that converge the system are given by,

$$\Delta P_p = \sum_{q=1}^{z} \Delta P_{pq} \tag{9}$$

Finally, the cost function Φ_p that is to be minimized is expressed as the summation of product of segment generations, cost factors and uncertainty factor $b_{pq,l}$ given by,

$$\Phi_p = min\left\{ C_{loss,p} \right\} = min\left\{ \left[\sum_{q=1}^{z} \left(\sum_{i=1}^{l} c_{pq,i} b_{pq,i} x_{pq,i} \right) \right] \right\} \tag{10}$$

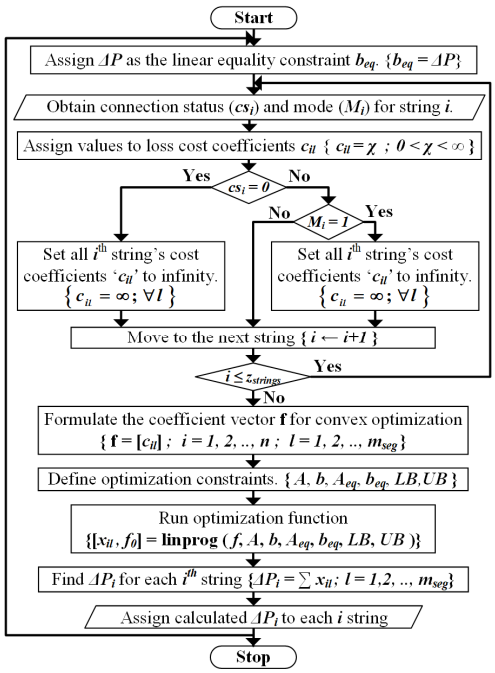


Fig. 3. Flowchart illustrating the execution of the OPA module.

$$C_{loss} = \begin{bmatrix} c_{12,1}b_{12,1}x_{12,1} + c_{12,2}b_{12,2}x_{12,2} + \ldots\ldots\ldots + c_{1z,l}b_{1z,l}x_{1z,l} \\ +\ldots \\ +c_{p1,1}b_{p1,1}x_{p1,1} + \ldots + c_{pq,l}b_{pq,l}x_{pq,l} + \ldots + c_{pz,l}b_{pz,l}x_{pz,l} \\ +\ldots \\ +c_{n1,1}b_{n1,1}x_{n1,1} + \ldots\ldots\ldots\ldots\ldots\ldots + c_{nz,l}b_{nz,l}x_{nz,l} \end{bmatrix} \tag{11}$$

The OPA module minimizes (10) using (11) to determine next instance optimal power allocations to GFL inverters, in response to assigned ΔP by following the flowchart in Fig. 3.

B. Proposed SR-CMS Control

The proposed SR-CMS control scheme uses a meshed communication network to enhance the resiliency of the PEDG against inverter's faulted controller or intentional disturbances. This meshed communication network is indicated by the blue dashed lines connecting each string inverter with its neighbors in Fig. 1.a. Each string inverter is considered a member agent and is modeled as a node. It is worth noting that the terms 'inverter' and 'agent' are interchangeably used here. In the event of a faulted GFM agent's controller, its power stage is disconnected from the PCC. However, this causes loss of PCC *V-f* references essential for the GFL agents and system loads. To avoid this, the SR-CMS mechanism is deployed on each agent's secondary controller. This mechanism exchanges status update packets between all neighboring agents to dynamically elect the next GFM inverter as discussed below.

C. Proposed SR-CMS mechanism: Packet Generation

To facilitate network visibility, a status update packet m_{ij} is produced by agent 'j' and shared to all its neighbors.

$$m_{ij} = [f_j, M_j, P_{res,j}, opt.p_j] \tag{12}$$

Here, (12) represents the status update packet shared by agent j with every neighboring agent i. f_j denotes agent j's fault status which is set to 1 if a fault is detected at its PCC. The M_j bit indicates j's operation mode, in GFM ($M_j = 1$) or GFL ($M_j = 0$). Next, P_{resj} signifies the available power reserve in terms of

This work is licensed under a Creative Commons Attribution 4.0 License. For more information, see https://creativecommons.org/licenses/by/4.0/

This article has been accepted for publication in IEEE Transactions on Industrial Electronics. This is the author's version which has not been fully edited and content may change prior to final publication. Citation information: DOI 10.1109/TIE.2023.3262866

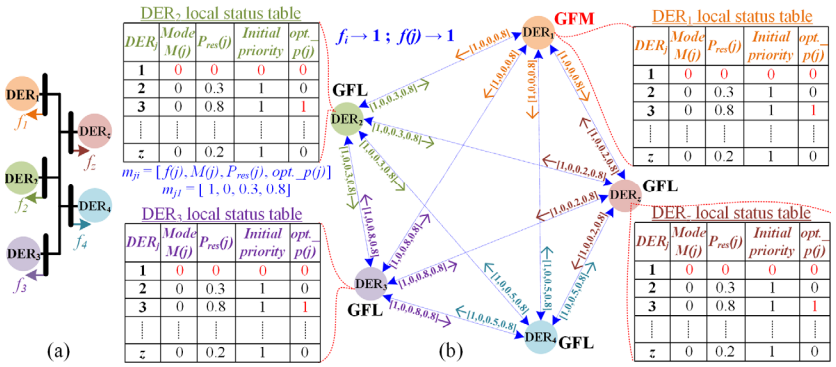


Fig. 4. Proposed SR-CMS mechanism: packet-based coordination between DERs (a) power stage, (b) communication graph.

percentage of the total capacity. This value is regulated by agent j's primary controller and depends on available power reserve in the hybrid dc source bound by the operation set-point, MPP power, BESS's SoC, etc. Finally, '$opt.P_j$' field represents the global optimized priority which is determined by a consensus between all agents. Consensus procedure is explained in next sub-sections. During an event, the agent with 'P_{resj}' matching the '$opt.P_j$' in its local status table is elected as the next GFM.

D. Proposed SR-CMS: Rank-based Mechanism

Fig. 4 shows a graphical representation of the cluster, consisting of one GFM and four GFL inverters. To maintain stable operation when a GFM fails, the rank-based approach is deployed. Consider N agents in a cluster. An initial rank $R_{0,i}$ is assigned to the agents based on their available power reserve so that each agent has a unique identification number given by,

$$R_{0,i} = (id)_i N \;;\; i = (1,...,5) \;;\; N = (1,...,i) \tag{13}$$

Here, i represents total number of available agents and N provides the number of integers required for initial rankings. As discussed previously, all communications among agents are through exchanged packets. For a faulted GFM j, as the error between PCC voltage magnitude V_{pcc} and threshold $V_{pcc,th}$ crosses tolerance ε_{vpcc}, and as error between frequency f_g and threshold $f_{g,th}$ crosses tolerance ε_{fg}, f_i bit is set to 1 by,

$$err\left(V_{pcc}\right) = \left|V_{pcc} - V_{pcc,th}\right| \Rightarrow \begin{cases} f_i = 1 & if \quad err\left(V_{pcc}\right) > \varepsilon_{vpcc} \\ f_i = 0 & if \quad err\left(V_{pcc}\right) \le \varepsilon_{vpcc} \end{cases} \tag{14}$$

$$err\left(f_g\right) = \left|f_g - f_{th}\right| \Rightarrow \begin{cases} f_i = 1 & if \quad err\left(f_g\right) > \varepsilon_{fg} \\ f_i = 0 & if \quad err\left(f_g\right) \le \varepsilon_{fg} \end{cases} \tag{15}$$

The tolerance values for amplitude ε_{vpcc} and frequency ε_{fg} are designed by system operator. The '$opt.p_i$' in (11) represents the next available agent to take over the GFM role. Equation (16) uses the fault status from (14) and (15), available power reserve of each agent and '$opt.p_i$' at instance '$k-1$' to select the most viable candidate inverter as the next GFM agent at instance k via the established priority function as,

$$\begin{aligned} opt.p_{i,k} &= opt.p_{i,k-1}\left(1 - f_{i,k-1}\right) + \left[\max\left(P_{res,i,k-1}\right)\right] f_{i,k-1} \\ M_{i,k} &= prior_{i,k}\left(opt.p_{i,k}\right) \end{aligned} \tag{16}$$

E. Proposed SR-CMS Mechanism

The proposed SR-CMS mechanism provides full visibility of the entire cluster to each of its agent. The initialization process assigns initial priorities to each agent based on their generation capacities. Based on the results of the rank-based LO, the GFM agent is elected, while other agents operate in GFL. Following the initialization process, each agent in the cluster periodically broadcasts a status update packet to all neighboring agents. The execution flow of the proposed SR-CMS mechanism is illustrated in Fig. 5. Under normal conditions, consider agent j is GFM, while other agents operate in GFL mode with no disturbances in the system. Agent j

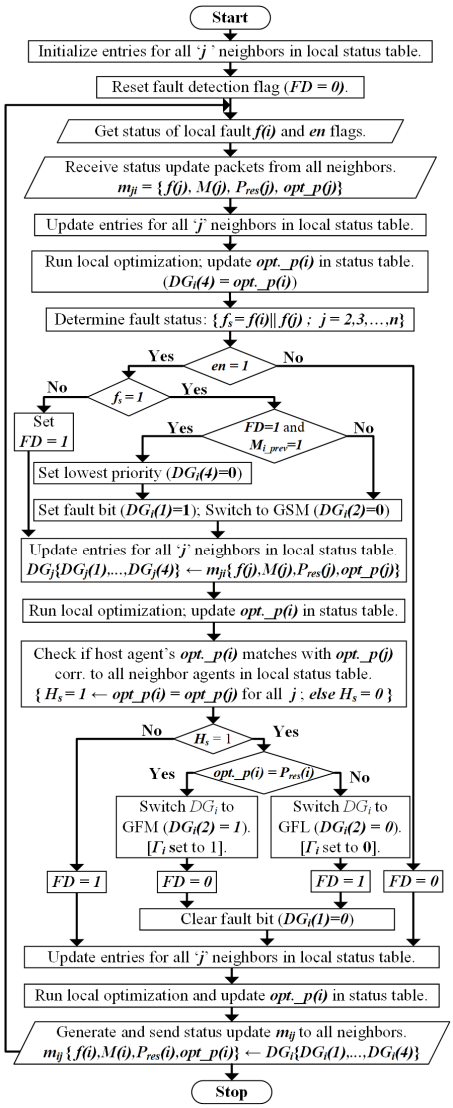


Fig. 5. Flowchart for execution of proposed SR-CMS algorithm.

This work is licensed under a Creative Commons Attribution 4.0 License. For more information, see https://creativecommons.org/licenses/by/4.0/

This article has been accepted for publication in IEEE Transactions on Industrial Electronics. This is the author's version which has not been fully edited and content may change prior to final publication. Citation information: DOI 10.1109/TIE.2023.3262866

broadcasts a status update packet at instance k as $m_{ij} = [0,1,0.9,0.9]$. Here the packet signifies that agent j is in GFM and maintains a power reserve of 0.9. Furthermore, it indicates that no fault has been detected at j's PCC and '$opt.p_j$' is 0.9. Accordingly, all neighbors update j status entry in their local update tables. In response, all neighbors send a status update packet to agent j with their updated P_{resj} and '$opt.P_j$' values.

When a GFL operating agent 'k' fails, the secondary controller disregards its binary factor Γ_k value, sets its connection status 'cs_k' to 0, and disconnects it from the PCC. Moreover, the secondary controller also flags the failed GFL 'k' by setting its '*Initial priority*' to 0 and its '$P_{res,k}$' to 0 to exclude it from the next candidate GFM selection process. This ensures that the next potential GFM candidate is not a faulty GFL agent.

Similarly, when a GFM agent 'j' fails, the PCC *V-f* limit violation is detected by the fault detection module in the proposed SR-CMS secondary controller. The secondary controller then disregards the value of binary factor Γ_j and disconnects the agent 'j' from its PCC. Furthermore, the mode bit M_j is set to 0 in agent j's local status table. Also '*Initial priority*' is set to 0, '$P_{res,j}$' is set to 0 (as evident from the control flow in Fig. 5) and '$opt.p_j$' is updated to new value obtained from LO (see Fig. 4). Agent 'j' now broadcasts the updated packet $m_{ij} = [1,0,0.0,0.8]$; conveying its fault status to neighboring agents. The f_i bit is set to 1 and mode bit m_j is set to 0 indicating inability to operate as GFM. Subsequently, all neighboring agents flag the agent j and run LO to find new $opt.p_i$. Agent 'j' uses the status update packets received from all neighbors to update its local status table and determine new $opt.p_i$ as indicated in the control flowchart in Fig. 5. This process of update exchange repeats and synchronization is complete when all the entries of *opt_p(j)* in agent j's local status table has the same homogenized priority values. After synchronization is attained, all agents are fully aware of their neighbor's status and the next eligible candidate takes over as the next GFM. Thus, agents are aware of their neighbor's status.

To elect the next GFM candidate, each agent i checks if its *Initial priority(i)* matches the homogenized *opt_p(i)*. If the *Initial priority(i)* matches the *opt_p(i)*, agent i's binary factor Γ_i will be set to 1 and this will cause the i^{th} agent to transit to GFM operation mode while other agents operate in GFL. This ensures at least one agent operates in GFM at any instance.

IV. Simulation Case Studies and Discussion

To illustrate the efficacy of proposed autonomous controller, three case scenarios have been investigated in MATLAB Simulink environment with five distributed energy resources (DER)s connected to PCC and feeding their local loads in an islanded PEDG cluster. The islanded PEDG cluster consist of one GFM inverter and four GFL inverters. System specifications for GFM and GFL inverters are provided in the Table II.

- Case Study 1 demonstrates the undesirable operation of the PEDG in the absence of proposed control.
- Case Study 2 illustrates the efficiency of the proposed SR-CMS mechanism in restoration of PCC *V-f* without the proposed SC based frequency restoration.

Table II. System specifications and component parameters

Symbol	Parameter	Value
z	Strings per cluster	5
P_{GFM}	GFM string's max. output power	22.06 kW
P_{GFL}	GFL string's max. output power	10.4 kW
f_{sw}	SCC's switching frequency	10 kHz
C_{dcl}	SCC's output-side capacitance	600 µF
$V_{dcl,ref}$	Reference DC-link voltage	650 V
$f_{inv,sw}$	GCI's switching frequency	28 kHz
L_{in}	GCI's inverter-side filter inductance	1.3 mH
C_f	GCI's filter capacitance	80 µF
R_d	Filter capacitor's damping resistance	0.1 Ω
L_g	Grid-side filter inductance	1 mH
$V_{g,rms}$	RMS grid voltage	208 V
f_g	Line frequency	60 Hz

- Case Study 3 illustrates the proposed autonomous control's ability to timely restore the frequency by dynamically assigning new set-points to GFL inverter when a GFM inverter is faulted and a steep fluctuation in loading occurs.

A. Case Study 1: Operation in absence of proposed control scheme

Case study 1 illustrates a system of one droop-based GFM inverter and several GFL inverters operating in the absence of the proposed SR-CMS control scheme. The cluster comprises of 5 DERs with DER_1 operating in GFM and maintaining the PCC *V-f* while the other inverters are operating in GFL. Initially, all the DERs are feeding their local loads and DER_1 regulates the frequency to 60 Hz as seen in Fig. 6(a) while feeding the system load of 11.5 kW in Fig. 6(b). In absence of the proposed control scheme, PEDG is highly susceptible to intentional and unintentional disturbances due to steep load variations or other potential anomalies or failures.

At t = 5 s, the DER_1 controller fails. At this instance, P_{DER1} instantly drops to 0 W and the load power (P_L) drops as well indicating an undesirable loss of load. The frequency regulation

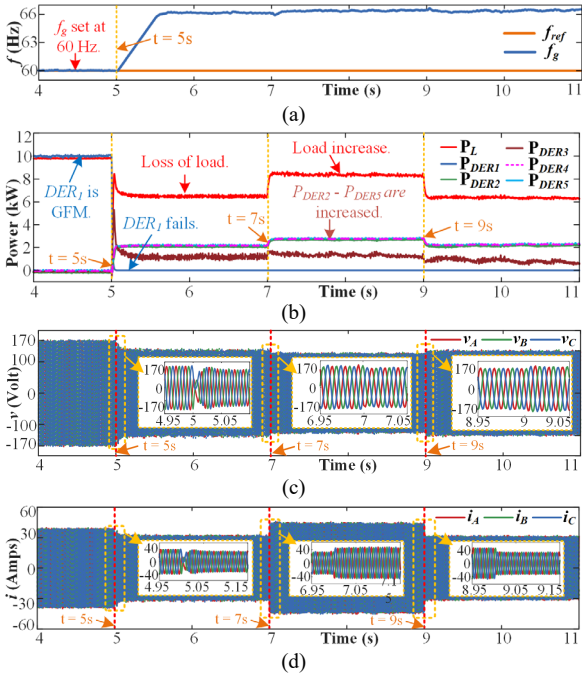


Fig. 6. Case study 1: GFM in conventional PEDG fails at t = 5 s followed by step loading: (a) frequency, (b) active powers, (c) PCC voltages and (d) load current; violation of grid voltage/frequency bounds.

This work is licensed under a Creative Commons Attribution 4.0 License. For more information, see https://creativecommons.org/licenses/by/4.0/

This article has been accepted for publication in IEEE Transactions on Industrial Electronics. This is the author's version which has not been fully edited and content may change prior to final publication. Citation information: DOI 10.1109/TIE.2023.3262866

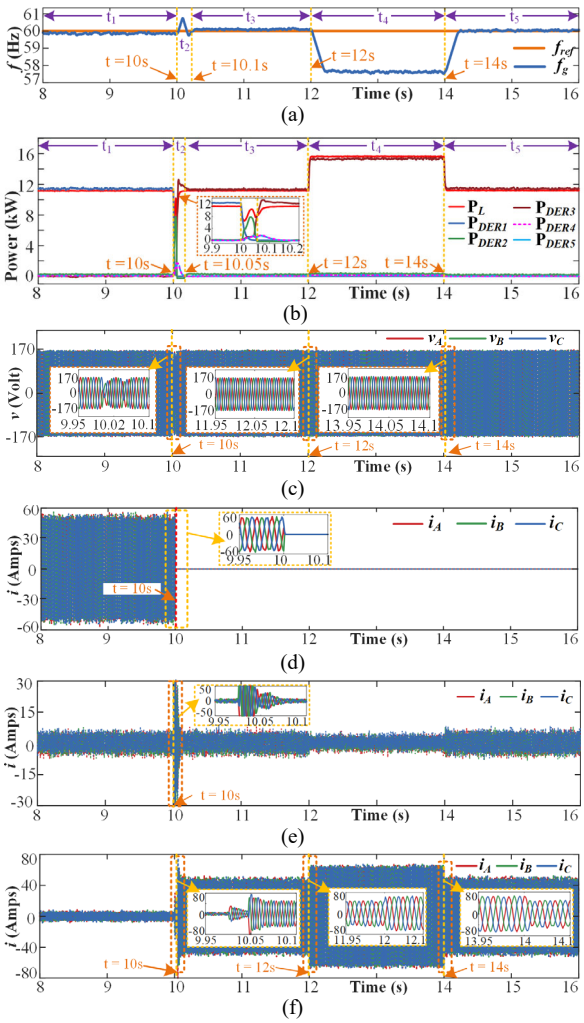


Fig. 7. Case Study 2: faulted GFM DER_1 at t = 10 s and DER_2 at t = 10.1 s: (a) frequency, (b) active powers, (c) PCC voltage (d) DER_1 output current, (e) DER_2 output current and (f) DER_3 output currents illustrating transition of GFM role from DER_1→ DER_2→ DER_3 followed by load disturbances.

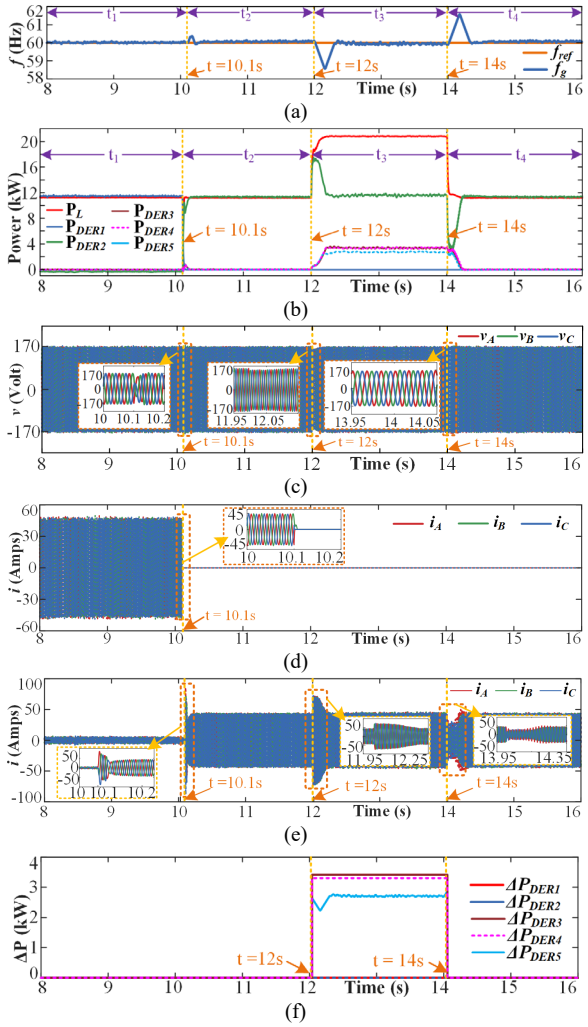


Fig. 8. Case Study 3: faulted GFM at t = 10.1 s and load disturbances between t = 12 s and t = 14 s: (a) Frequency, (b) active powers, (c) PCC voltages, (d) DER_1 output currents (e) DER_2 output currents and (f) real-time ΔP allocations for the timely restoration of PCC *V-f* for stable system operation due to the proposed autonomous control scheme with SC.

is lost as it deviates to about 66 Hz (see Fig. 6(a)). Moreover, the PCC voltage drops below the nominal value after t = 5 s in Fig. 6(c). Under such conditions, system loading is varied by 5kW in between t = 7 s and t = 9 s. This causes PCC voltage to further drop below the nominal value as seen in Fig. 6(c). The load current also varies proportionately in Fig. 6(d). However, in this case study a clear violation of *V-f* limits is observed which would trigger relays and disconnect the inverters from the network.

B. Case Study 2: Validation of proposed control without SC

To ensure that PCC voltage is regulated, and uninterrupted power is always fed to loads, the proposed SR-CMS mechanism has been deployed in the PEDG network. Initially, DER_1 is assigned the GFM role considering its highest initial priority of 0.9. DER_2 to DER_5 are regulated in GFL mode. For simplicity in explanation, the time duration is divided into five intervals (t_1 to t_5) as shown in the results in Fig. 7(a) - Fig. 7(f).

Initially, the system is stable in time interval t_1 and frequency is maintained at 60 Hz as shown in Fig. 7(a). DER_1 feeds the 11.5 kW system load (blue plot in Fig. 7(b)); while DER_2 to DER_5 are synchronized with PCC voltage (see Fig. 7(c)). Their power injection (P_{DER2} to P_{DER5}) into the PEDG during t_1 interval is 0 W. At t = 10 s, the GFM DER_1 fails, indicated by P_{DER1} (blue plot in Fig. 7(b)) dropping to 0 W and its output current falling to 0 A in Fig. 7(d). As the fault detection module detects a violation of PCC *V-f*, the SR-CMS mechanism triggers a fault and DER_2 with the next highest initial priority is elected as the next GFM in t_2. DER_2 switches mode to GFM and starts regulating the PCC's *V-f*. It also serves the load which was previously served by DER_1. This is evident from the brown plot in the zoomed window of Fig. 7(b). A proportionate increase in the DER_2 output currents is observed in Fig. 7(e) in t_2. However, due to insufficient instantaneous available power, DER_2 cannot meet the load requirements and hence fails (P_{DER2} → 0 W) at about t = 10.1 s. Instantly, the SR-CMS mechanism re-elect's DER_3 as the next GFM at the start of t_3. DER_3's output currents also increase as shown in Fig. 7(f).

Next, a step increase of 5kW in system load is introduced at time instance t_4 from t = 12 s to t = 14 s. DER_3 increases its output power P_{DER3} (brown plot in t_4 of Fig. 7(b)). However, this causes the frequency to deviate to 59 Hz. Thus, frequency bounds could be violated leading to undesirable operation.

This work is licensed under a Creative Commons Attribution 4.0 License. For more information, see https://creativecommons.org/licenses/by/4.0/

This article has been accepted for publication in IEEE Transactions on Industrial Electronics. This is the author's version which has not been fully edited and content may change prior to final publication. Citation information: DOI 10.1109/TIE.2023.3262866

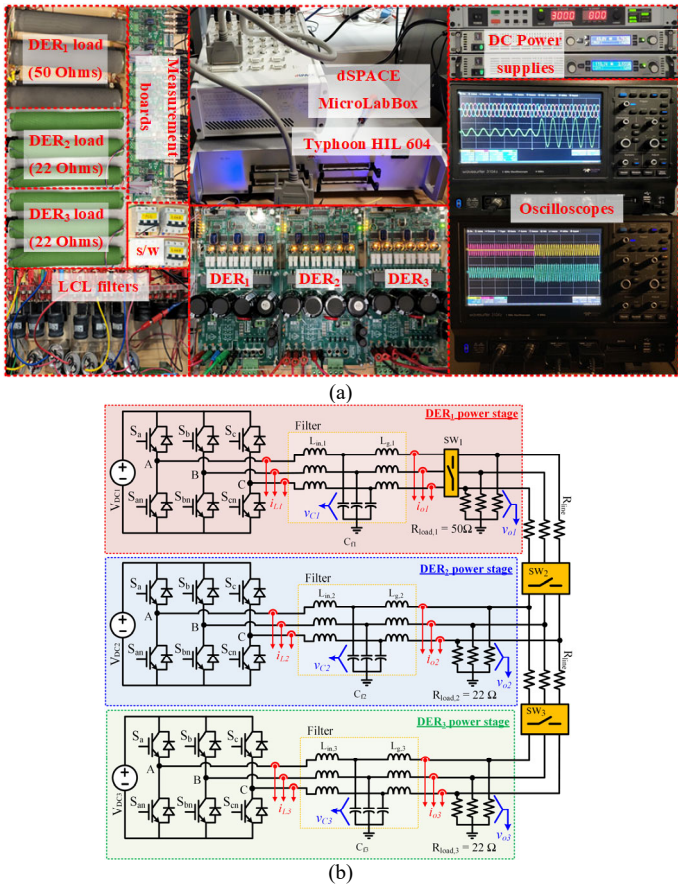


Fig. 9. (a) Experimental hardware setup of three DERs and (b) their connection topology in the microgrid testbed

C. *Case Study 3: Validation of proposed autonomous control scheme with the SC*

To ensure the real-time mitigation of frequency excursions during an event, the proposed SC D-PAO based frequency restoration in the proposed autonomous control is incorporated. This ability of the proposed control to timely restore frequency is demonstrated here. The performance of the system in response to a failed GFM inverter followed by load disturbances is illustrated in Fig. 8(a) – Fig. 8(f).

Initially, during interval t_1, frequency is held at 60 Hz (Fig. 8(a)) and DER_1 supports the 11.5 kW system load (Fig. 8(b)). At t = 10.1 s, the GFM operating DER_1 fails and is replaced by DER_2 as next GFM by the SR-CMS mechanism. Thus, P_{DER2} indicated by green plot increases in interval t_2 of Fig. 8(b). The PCC voltage remains almost uninterrupted as seen in Fig. 8(c), while the collapse of DER_1 and rise of DER_2 power is also evident from their respective output currents in Fig. 8(d) and Fig. 8(e). At t = 12 s, the system load is increased by 10 kW to simulate steep load fluctuations.

Initially, GFM DER_2 feeds this additional load by increasing its power output. This leads to a drift in the frequency as seen in interval t_3 of Fig. 8(a). This drift in frequency is detected by SC and it increases the power allocations ΔP to all GFL operating DERs (in Fig. 8(f)); to serve the additional load. This is evident from the rise in P_{DER3}, P_{DER4} and P_{DER5} during t_3 interval in Fig. 8(b). Consequently, P_{DER2} decreases almost immediately, and the frequency is returned to 60 Hz nominal in a timely manner (in less than 0.15 s); thereby satisfying the timing norms set by the grid standards. A similar type of fast frequency restoration is seen at the end of instance t_4 when the system loading is decreased back to 11.5 kW.

Thus, the proposed autonomous control can maintain stable operation of the PEDG while mitigating impacts of faulted GFM inverters as well as other disturbances related to system loading.

V. Experimental Validation

The proposed autonomous control scheme is validated experimentally on a system of three inverters representing a small-scale network of GFM and GFL DERs shown in Fig. 9(a). The connection topology of the three DERs is shown in Fig. 9(b). The primary and secondary level controllers for DER_1 and DER_2 were implemented on a dSPACE MicroLab box while the primary and secondary level controllers for DER_3 and the proposed SC (consisting of ΔP estimator and OPA module) implemented on a Typhoon HIL 604. The power allocation set-points for DER_1, DER_2 and DER_3 are estimated by the SC implemented in Typhoon HIL 604 are communicated through serial communication between the Typhoon 604 and the dSPACE. Each DER is equipped with an LCL filter whose component values are provided in Table. II. Programmable dc supplies are used to simulate the hybrid dc sources. Initially, DER_1 is regulated in GFM mode serving system load of 50 Ω, while DER_2 and DER_3 operate in GFL mode serving their local loads of 22 Ω each and are also connected to the DER_1 via the PCC contactor switches.

The line frequency is plotted in Fig. 10(a) while the output power profiles of each DER for the entire duration of the hardware testing are shown in Fig. 10(b). Furthermore, the PCC voltage phase-a is represented by the yellow plot while the phase-a currents of DER_1, DER_2 and DER_3 are represented by the red, green and blue plots respectively in the oscilloscope image in Fig. 10(c). Finally, the three phase PCC voltage is shown by the red, blue and yellow plots while the DER_2 phase-a current is shown in Fig. 10(d). At t = 9.2 s, the GFM operating DER_1 is lost due to an intentional failure to represent the scenario of loss of a GFM inverter. Thus, frequency and voltage regulation is lost, and frequency starts dropping from the 60 Hz nominal after time instance t_1 as observed in the Fig. 10(a). After the DER_1 is lost, its output power drops to zero after time instance t_1, represented by the blue plot in Fig. 10(b). This can also be verified from the DER_1's phase-a current dropping to 0 Amps after time instance t_1 (represented by red plot in Fig. 10(c)). Also, the three phase PCC voltages in Fig. 10(d) drops below the nominal after t_1. This violation of PCC *V-f* is detected by the fault detection modules in the secondary controllers of DERs. Furthermore, the fault status is also communicated to the secondary controllers of each DER internally. In the transition window between time instances t_1 and t_2 the DER_2 is switching its operation mode from GFL to GFM. As shown in post fault period, the PCC voltage is not being regulated momentarily. This also causes the DER_2 currents to be unregulated (green plot in Fig. 10(c) and Fig. 10(d)).

As the fault is verified by the DER_1's secondary controller, it sets its local priority to 0 to indicate its inability to serve as the next GFM. After confirmation of the fault status, the DER_2's

This work is licensed under a Creative Commons Attribution 4.0 License. For more information, see https://creativecommons.org/licenses/by/4.0/

This article has been accepted for publication in IEEE Transactions on Industrial Electronics. This is the author's version which has not been fully edited and content may change prior to final publication. Citation information: DOI 10.1109/TIE.2023.3262866

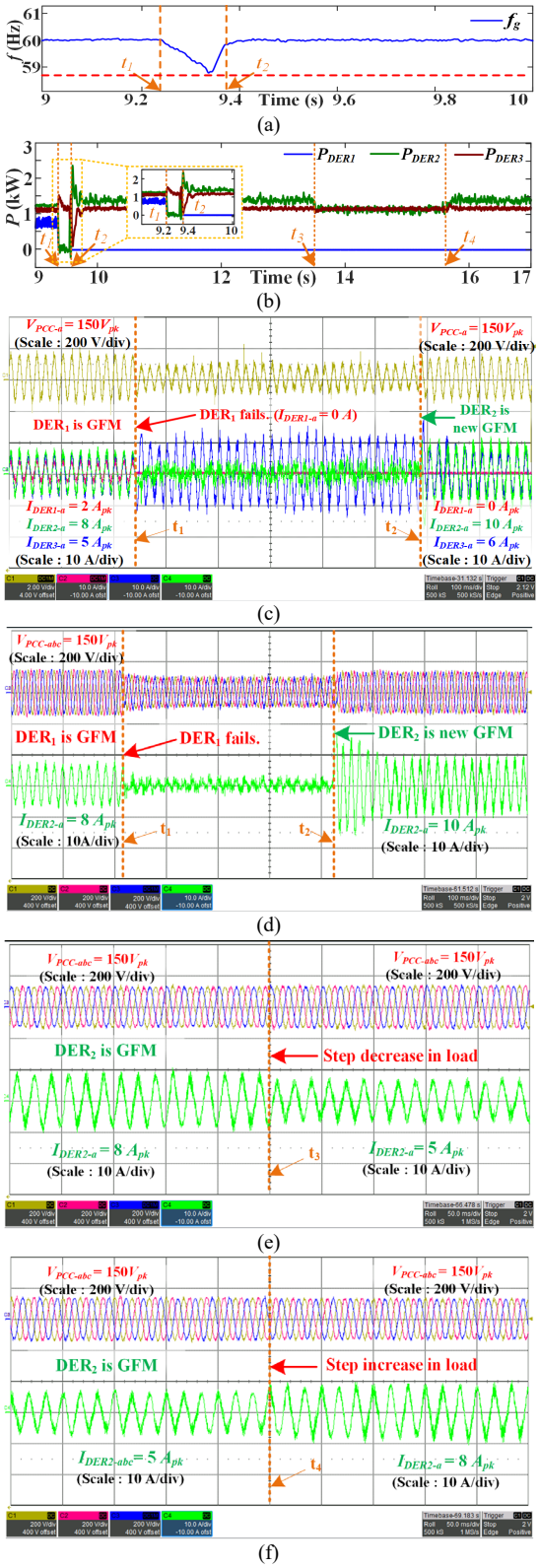


Fig. 10. Experimental results: DER_1, DER_2 and DER_3 connected at PCC, DER_1 is faulted, removed from the network at t = 9.2 s: (a) frequency, (b) power profiles, (c) PCC phase-a voltage and phase-a currents of all three DERs when DER_1 is lost and DER_2's transits to GFM in between t_1 and t_2, (d) three phase PCC voltages and DER_2 phase-a current when DER_1 is lost and DER_2's mode transition from GFL to GFM in about 0.4s between t_1 and t_2, (e) step decrease in system load and (f) step increase in system load where PCC *V-f* are maintained at their nominal values by newly elected GFM DER_2.

secondary control elects itself as the next GFM inverter while the DER_3's controller continues to operate in GFL mode based on the proposed SR-CMS scheme. Consequently, the DER_2's secondary control switches its operation mode from GFL to GFM smoothly in less than 250 ms after the PCC *V-f* limit violation is detected. The DER_2 now starts regulating the PCC *V-f* after time instance t_2. This can be validated by the PCC voltage magnitude returning to nominal after time instance t_2 in the oscilloscope waveforms seen in Fig. 10(c) and Fig. 10(d). Also, the line frequency is returned to nominal 60 Hz in about 250 ms by the newly elected GFM DER_2. This validates the operation of the proposed SR-CMS control scheme on small-scale hardware setup. The DER_2's output current phase-a (green plot in Fig. 10(c) and Fig. 10(d)) also increases proportionately due to the overall increase in its load from 22 Ω to 15.28 Ω.

Next, to verify the operation of the DER_2 as the newly appointed GFM, the system load of 30 Ω is disconnected from the PCC at instance t_3. Thus, the load served by DER_2 drops to 22 Ω. It can be observed that the three phase PCC voltage (red, blue and yellow plots in Fig. 10(e)) is maintained at the nominal even after the load disturbance occurred at time instance t_3, while the DER_2's output current (green plots in Fig. 10(e)) decrease proportionately. Similarly, the GFM operating DER_2 regulates the PCC voltage to the nominal value (red, blue and yellow plots in Fig. 10(f)) while its output current increases proportionately after time instance t_4; when the 22 Ω load is reconnected at the PCC. Thus, the GFM operation of DER_2 after the mode transition is verified. These results verify the functionality of the proposed autonomous control scheme with the frequency restoration in a small-scale hardware testbed.

VI. Conclusion

An autonomous resilient control with self-ranking based coordinated mode selection and *V-f* restoration capabilities for a cluster of inverters in a PEDG is proposed. During load disturbances, the OPA based SC is capable of restoring frequency within the allowable time bounds. The droop-based ΔP estimator accurately estimates the differential power required to restore the frequency while the optimal power allocator module minimizes the incurred power losses while ensuring timely restoration of frequency. Moreover, the use of SC eliminates the dependency on the droop based complex coordination to attain power sharing among interconnected inverters. Furthermore, the proposed SR-CMS mechanism enables instantaneous restoration of the PCC *V-f* if a GFM inverter's controller is faulted or compromised. The case studies and results validate the ability and robustness of the proposed scheme to withstand during an event. Furthermore, the experimental results obtained from hardware testing on the small-scale testbed validate the feasibility of the proposed control scheme. Thus, the proposed control scheme enhances the resiliency of network of GFL and GFM inverters in PEDG.

Acknowledgment

This publication was made possible by grants NPRP12C-33905-SP-213 and NPRP12C-33905-SP-220 from the Qatar National Research Fund (QNRF is a member of Qatar

This work is licensed under a Creative Commons Attribution 4.0 License. For more information, see https://creativecommons.org/licenses/by/4.0/

This article has been accepted for publication in IEEE Transactions on Industrial Electronics. This is the author's version which has not been fully edited and content may change prior to final publication. Citation information: DOI 10.1109/TIE.2023.3262866

Foundation). The statements made herein are solely the responsibility of the authors.

REFERENCES

[1] A. Khan, M. Hosseinzadehtaher, M. B. Shadmand, S. Bayhan, and H. Abu-Rub, "On the stability of the power electronics-dominated grid: A new energy paradigm," *IEEE Ind. Electronics Magazine,* vol. 14, no. 4, pp. 65-78, 2020.

[2] Y. Lin *et al.*, "Research roadmap on grid-forming inverters," National Renewable Energy Lab.(NREL), Golden, CO (United States), 2020.

[3] S. D'silva, M. Shadmand, S. Bayhan, and H. Abu-Rub, "Towards grid of microgrids: Seamless transition between grid-connected and islanded modes of operation," *IEEE Open Journal of the Industrial Electronics Society,* vol. 1, pp. 66-81, 2020.

[4] M. E. T. Souza and L. C. G. Freitas, "Grid-Connected and Seamless Transition Modes for Microgrids: An Overview of Control Methods, Operation Elements, and General Requirements," *IEEE Access,* vol. 10, pp. 97802-97834, 2022.

[5] B. K. Poolla, D. Groß, and F. Dörfler, "Placement and implementation of grid-forming and grid-following virtual inertia and fast frequency response," *IEEE Trans. P. Systems,* vol. 34, no. 4, pp. 3035-3046, 2019.

[6] R. H. Lasseter, Z. Chen, and D. Pattabiraman, "Grid-Forming Inverters: A Critical Asset for the Power Grid," *IEEE Journal of Emerging and Selected Topics in Power Electronics,* vol. 8, no. 2, pp. 925-935, 2020.

[7] J. Wang and G. Saraswat, "Study of Inverter Control Strategies on the Stability of Low-Inertia Microgrid Systems," National Renewable Energy Lab.(NREL), Golden, CO (United States), 2022.

[8] Y. Qi, H. Deng, J. Fang, and Y. Tang, "Synchronization Stability Analysis of Grid-Forming Inverter: A Black Box Methodology," *IEEE Trans. Ind. Electron.,* vol. 69, no. 12, pp. 13069-13078, 2022.

[9] D. Y. Yamashita, I. Vechiu, and J.-P. Gaubert, "A review of hierarchical control for building microgrids," *Renewable and Sustainable Energy Reviews,* vol. 118, p. 109523, 2020/02/01/ 2020.

[10] T. Khalili and A. Bidram, "Distributed control approaches for microgrids," in *Microgrids*: Springer, 2021, pp. 275-288.

[11] H. S. Bidgoli and T. V. Cutsem, "Combined Local and Centralized Voltage Control in Active Distribution Networks," *IEEE Trans. P. Sys.,* vol. 33, no. 2, pp. 1374-1384, 2018.

[12] C. Samende, S. M. Bhagavathy, and M. McCulloch, "Power Loss Minimization of Off-Grid Solar DC Nano-Grids—Part I: Centralized Control Algorithm," *IEEE Trans. S. Grid,* vol. 12, pp. 4715-4725, 2021.

[13] A. Singhal, T. L. Vu, and W. Du, "Consensus Control for Coordinating Grid-Forming and Grid-Following Inverters in Microgrids," *IEEE Transactions on Smart Grid,* vol. 13, no. 5, pp. 4123-4133, 2022.

[14] S. M. Mohiuddin and J. Qi, "Optimal Distributed Control of AC Microgrids With Coordinated Voltage Regulation and Reactive Power Sharing," *IEEE Trans. S. Grid,* vol. 13, no. 3, pp. 1789-1800, 2022.

[15] M. Chamana, B. H. Chowdhury, and F. Jahanbakhsh, "Distributed Control of Voltage Regulating Devices in the Presence of High PV Penetration to Mitigate Ramp-Rate Issues," *IEEE Trans. S. Grid,* vol. 9, no. 2, pp. 1086-1095, 2018.

[16] M. Bell, F. Berkel, and S. Liu, "Real-Time Distributed Control of Low-Voltage Grids With Dynamic Optimal Power Dispatch of Renewable Energy Sources," *IEEE Trans. Sustainable Energy,* vol. 10, no. 1, 2019.

[17] T. V. Vu, S. Paran, F. Diaz-Franco, T. El-Mezyani, and C. S. Edrington, "An Alternative Distributed Control Architecture for Improvement in the Transient Response of DC Microgrids," *IEEE Trans. Ind. Electron.,* vol. 64, no. 1, pp. 574-584, 2017.

[18] X. Li, D. Hui, and X. Lai, "Battery energy storage station (BESS)-based smoothing control of photovoltaic (PV) and wind power generation fluctuations," *IEEE Trans. sus. energy,* vol. 4, no. 2, pp. 464-473, 2013.

[19] D. Curto *et al.*, "Grid Stability Improvement Using Synthetic Inertia by Battery Energy Storage Systems in Small Islands," *Energy,* p. 124456, 2022.

[20] U. Markovic, O. Stanojev, P. Aristidou, and G. Hug, "Partial grid forming concept for 100% inverter-based transmission systems," in *2018 IEEE Power & Energy Society General Meeting (PESGM)*, 2018.

[21] J. W. Simpson-Porco, Q. Shafiee, F. Dörfler, J. C. Vasquez, J. M. Guerrero, and F. Bullo, "Secondary frequency and voltage control of islanded microgrids via distributed averaging," *IEEE Trans. Ind. Electron.,* vol. 62, no. 11, pp. 7025-7038, 2015.

[22] M. Eskandari *et al.*, "Active power sharing and frequency restoration in an autonomous networked microgrid," *IEEE Trans. P. Systems,* vol. 34, no. 6, pp. 4706-4717, 2019.

[23] H. Han *et al.* , "Review of power sharing control strategies for islanding operation of AC microgrids," *IEEE Trans. S. Grid,* vol. 7, no. 1, pp. 200-215, 2015.

[24] S. D'silva *et al.*, "Coordinated Power Reserve Control of PV Sources For Frequency Restoration in Power Electronics Dominated Grid," in *IEEE SGRE*, 2022.

[25] R. Guzman, L. G. de Vicuña, A. Camacho, J. Miret, and J. M. Rey, "Receding-horizon model-predictive control for a three-phase VSI with an LCL filter," *IEEE Trans. Ind. Electron.,* vol. 66, pp. 6671-6680, 2018.

[26] K.-W. Lao, W. Deng, J. Sheng, and N. Dai, "PQ-coupling strategy for droop control in grid-connected capacitive-coupled inverter," *IEEE Access,* vol. 7, pp. 31663-31671, 2019.



Silvanus D'silva (S'18) received his Bachelors in Electronics and Telecommunication Engineering from University of Mumbai, India (MU). He obtained his M.Sc. in Electrical Engineering from Kansas State University in 2020. He worked as a graduate researcher in the TEES lab at the Smart Grid Centre in Texas A&M University at Qatar from January 2021 to August 2021. Currently, he is pursuing his Ph.D. degree in Electrical Engineering from University of Illinois Chicago. He joined the IPEG Research Group in August 2021.



Alireza Zare (S'19) has received his B.Sc degree in electrical engineering with a focus on power engineering from Shiraz University, Shiraz, Iran, in 2017 . He has received his MS degree at Washington State University, Vancouver, WA, USA in 2020. He has joined the electrical and computer engineering department at the University of Illinois Chicago as a PhD student starting fall 2021.



Mohammad B. Shadmand (M'15-SM'20) received the Ph.D. degree in electrical engineering from Texas A&M University, College Station, TX, USA, in 2015. From 2017 to 2020, he was an Assistant Professor with the Department of Electrical and Computer Engineering, Kansas State University, Manhattan, KS, USA. Since 2020, he is an Assistant Professor with the University of Illinois at Chicago, IL, USA. Dr. Shadmand was awarded Michelle Munson Serban Simu Keystone Research Scholar, Kansas State University in 2017. He was awarded the 2019 IEEE Myron Zucker Faculty-Student Research Grant. He has awarded multiple best paper awards at different IEEE conferences. He is the General Co-Chair of 50th Annual Conference of the IEEE Industrial Electronics Society (IECON 2024), Chicago, IL. He serves as Associate Editor of IEEE Transactions on Industrial Electronics, IEEE Transactions on Industry Application, and IET Renewable Power Generation.

This work is licensed under a Creative Commons Attribution 4.0 License. For more information, see https://creativecommons.org/licenses/by/4.0/

This article has been accepted for publication in IEEE Transactions on Industrial Electronics. This is the author's version which has not been fully edited and content may change prior to final publication. Citation information: DOI 10.1109/TIE.2023.3262866



Sertac Bayhan (Senior Member, IEEE) received the bachelor's degree and the M.S. and Ph.D. degrees in electrical engineering from Gazi University, Ankara, Turkey, in 2008 and 2012, respectively. He is currently working as a Senior Scientist with the Qatar Environment and Energy Research Institute (QEERI). He is a Faculty Member with the rank of an Associate Professor with the Sustainable Division, College of Science and Engineering, Hamad Bin Khalifa University. He has acquired $13M in research funding and published more than 170 papers in mostly prestigious IEEE journals and conferences. He is also the coauthor of two books and five book chapters. He was a recipient of many prestigious international awards.



Haitham Abu-Rub (Fellow, IEEE) received the two Ph.D. degrees. He worked at many universities in many countries, including Poland, Palestine, USA, Germany, and Qatar. Since 2006, he has been with Texas A&M University at Qatar. For five years, he has served as the Chair for the Electrical and Computer Engineering Program, Texas A&M University at Qatar. He is currently working as the Managing Director with the Smart Grid Center. He has published more than 400 journal articles and conference papers, five books, and six book chapters. He has supervised many research projects on smart grid, power electronics converters, and renewable energy systems. His main research interests include electric drives, power electronic converters, renewable energy, and smart grid. He was a recipient of many national and international awards and recognitions. He was a recipient of the American Fulbright Scholarship, the German Alexander von Humboldt Fellowship, and many others.

This work is licensed under a Creative Commons Attribution 4.0 License. For more information, see https://creativecommons.org/licenses/by/4.0/